75^{th} International Astronautical Congress (IAC), Milano, Italy, 14-18 October 2024
Copyright © 2024 by the International Astronautical Federation (IAF). All rights reserved.

IAC–24–IAC-24-B4.IP.112.x91111

HERMES constellation for astrophysics: the thermal modeling and testing strategy for qualification

Matteo Quirino*, Lorenzo Capra†, Alice Dottori‡, Stefano Marinelli§, Stefano Silvestrini¶, Michéle Lavagnaand Roberto Bertacin††**

Abstract HERMES is a modular project composed by six 3U nanosatellites: the initial trio of Technology Pathfinder (TP) CubeSats receives funding from the Italian Ministry of University and Research (MUR) and the Italian Space Agency (ASI), while the subsequent triplet of Scientific Pathfinder (SP) satellites is supported by the European Union (EU) via an H2020-SPACE grant. Scheduled for launch in 2025, the project currently progresses through an advanced phase D. The primary objective of the HERMES initiative is to accurately localize bright astrophysical transients using triangulation techniques, via an advanced detector engineered by the National Institute of Astro Physics (INAF). This payload is highly susceptible to thermal conditions and temperature fluctuations, so it is critical to have a well-designed and efficient thermal subsystem for a high-scientific return. The robustness of the thermal subsystem design is rigorously assessed through a stringent AIV/AIT thermal vacuum (TVAC) testing, for de-risking purposes, at TAS-I facility. This classic testing approach, usually tailored for much bigger spacecrafts, simulates the extreme conditions of space, ensuring that the proposed passive thermal system can effectively regulate temperature variations and safeguard the satellite's components against potentially damaging thermal fluctuations. This methodology, mainly limited to bigger missions, is here proposed also for these nanosatellites. The test is performed placing the satellites on a jig, bolted onto an interface plate, both covered with Kapton to increase emissivity and manufactured at Politecnico di Milano. To have a very well-defined radiation environment during the test and ease the correlation of the test results, the satellite is surrounded by an aluminum box, covered with Kapton and sensorized with thermocouples. Data are parsed during both the non-operative and operative thermal cycles and are used to correlate the ESATAN model implemented to reproduce the TVAC test. This step is critical because it allows to ensure the model accurately reflects the satellite's behavior. This correlation process involves adjusting parameters within the thermal model, such as the thermal resistances to be defined for each conduction thermal exchange. Therefore, this operation enhances the model's predictive capabilities and enables more reliable future analyses with the improved and more accurate thermal links. Conclusively, testing the satellite in a thermal vacuum environment and subsequently correlating the model with the results are vital steps in ensuring the spacecraft's resilience and performance in the harsh conditions of space, thereby mitigating risks and augmenting mission success.
keywords: CubeSat, Thermal Model Correlation, Thermal Vacuum Test, ESATAN, Gamma Ray Burst.

1. Introduction

The HERMES (High Energy Rapid Modular Ensemble of Satellites) mission is thought as a constellation of six 3U CubeSats in Low Earth Orbit, featuring an innovative payload to detect the temporal emission of bright high-energy transients such as Gamma-Ray Bursts (GRBs). It is composed of two twin projects, each consisting of three satellites: HERMES Technological Pathfinder (HERMES-TP) funded by the Italian Space Agency (ASI) and HERMES Scientific Pathfinder (HERMES-SP) financed by the European Commission's H2020 project.

HERMES aims to demonstrate that it is possible to obtain an accurate and prompt localization of bright hard X-ray/soft gamma-ray transient such as GRBs [1]. At the same time, the mission wants to prove that it is possible to cut costs and the time-to-orbit by using nanosatellites mostly using off-the

*Politecnico di Milano, Italy, matteo.quirino@polimi.it
†Politecnico di Milano, Italy, lorenzo.capra@polimi.it
‡Politecnico di Milano, Italy, alice.dottori@polimi.it
§Politecnico di Milano, Italy, stefano2.marinelli@mail.polimi.it
¶Politecnico di Milano, Italy, stefano.silvestrini@polimi.it
**Politecnico di Milano, Italy, michelle.lavagna@polimi.it
††Italian Space Agency, Italy, roberto.bertacin@asi.it

Copyright © 2024 by the International Astronautical Federation (IAF). All rights reserved.

shelf components, which reduce the costs to 1-2 order of magnitude lower than that of standard space projects [1].

The whole mission involves the participation of several entities, among them there are Istituto Nazionale di Astrofisica (INAF), which is responsible for the scientific payload, and Politecnico di Milano (Polimi), in charge of the design of the service module. Polimi is in charge also for the payload integration and for the system assembly, integration and testing as well as all the coordination in the development of the mission ground segment [1].

The Department of Aerospace Science and Technology at Politecnico di Milano is responsible for designing, implementing, and testing all the CubeSat subsystems, including the Thermal Control Subsystem (TCS).

The performance of the TCS are checked by developing a Thermal Model of the CubeSat. Indeed, the spacecraft's Thermal Model must demonstrate that all components remain within their operational temperature range throughout the mission. This is essential for both the spacecraft's survival and the successful achievement of its scientific objectives.

To ensure the reliability of the Thermal Model, it must be validated by comparing its results with those of the Thermal Vacuum Test (TVAC). If the Thermal Model, under the same configuration and boundary conditions as the spacecraft during the TVAC test, produces consistent results, its accuracy can be trusted.

This work present the correlation of the thermal model of the HERMES-TP CubeSat with the results of the test campaign, ensuring that the model outcome accurately reflects the actual behavior of the spacecraft. The correlation is done using ESATAN, and the criteria for its success are specified in the ECSS-E-ST-31C. In the end with the correlated model the orbital thermal analyses are presented to show the actual final temperature field.

The paper is structured as follows: Sec.2 the HERMES CubeSat is presented, Sec.3 reports the Thermal Vacuum Test results, Sec.4 provides an insight of the ESATAN model, Sec.5 contains the correlation results and finally the updated thermal analyses are shown in Sec.6, the conclusions are in Sec.7.

2. Hermes Mission

The CubeSats will be launched in 2025 into sun-synchronous orbits at 550 km altitude. They will drift apart naturally, enabling the triangulation baseline for GRBs source localization. Each CubeSat is equipped with an Iridium transceiver for rapid data transmission, alerting observatories worldwide when a GRB is detected. The CubeSats are 3U in size (10x10x30 cm), with the Scientific Payload designed by the Istituto Nazionale di Astrofisica (INAF) on the top unit of the satellite. The payload performs high resolution spectral-timing analysis of long and short GRBs.

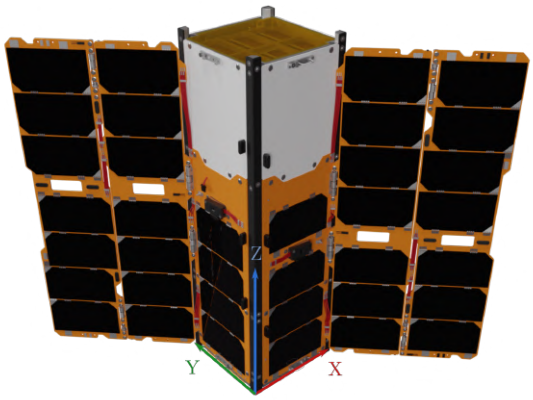

(a) Front

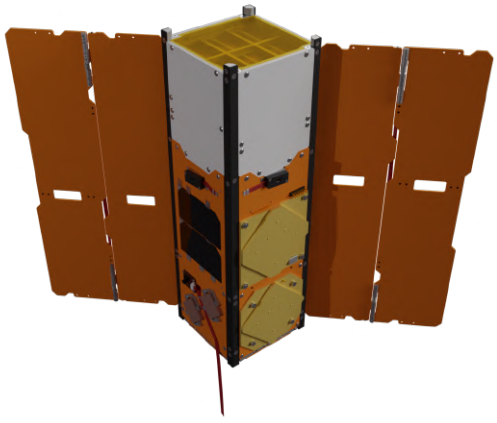

(b) Back

Fig. 1: HERMES CubeSat.

When a Gamma-Ray Burst (GRB) is detected, the CubeSat's estimated location and the detection

Copyright © 2024 by the International Astronautical Federation (IAF). All rights reserved.

timestamp are recorded to triangulate the GRB's direction with several degrees of accuracy. This accuracy depends on the GRB's characteristics and the configuration of the triplet observing the event.

The timing accuracy is ensured by a chip-scale atomic clock integrated into the Payload (PL), which is synchronized with GPS time through PPS synchronization. To maintain precise atomic clock timing, the component temperature must be kept above $-10\,^{\circ}$C.

For GRB detection and energy time history recording, the PL utilizes 120 Silicon Drift Detectors (SDDs) and 60 GAGG crystals, with each crystal paired with 2 SDDs. The SDDs are the core of the instrument and must operate below $-5\,^{\circ}$C. to minimize leakage current from on-orbit radiation damage, thus ensuring optimal spectroscopic performance and longevity.

To maintain these low temperatures, the PL's structural panels feature an Aeroglaze coating that reflects most sunlight and maximizes radiative heat emission in the infrared spectrum.

3. Thermal Vacuum Test

The process of correlating the thermal model relies on the data recorded during the test campaign, which is briefly described in this section. Some details are intentionally omitted, as a thorough description of the test is beyond the scope of this article.

The presented tests are carried out on the Protoflight Model (PFM) of the HERMES CubeSat (the first of the six CubeSat to be built), following the ECSS-E-ST-31C guidelines [2]. They are conducted at the Thales Alenia Space Italy (TAS-I) facility in Gorgonzola, using their Thermal Vacuum Chamber (TVAC).

3.1 *TVAC overview*

The TVAC at Thales Alenia Space Italy (TASI) facility in Gorgonzola has an available internal volume of 750(L)x600(P)x650(H) mm.

The mechanical connection between the HERMES CubeSat and the TVAC is possible due to an interface plate, manufactured by Polimi. It is designed such that it matches the pattern of the TASI-TVAC plate, allowing the integration of two satellites at the same time if needed, thus parallelizing the tests. Bolted on the interface plate there is a set of jigs, which is used to keep the satellite in place during the tests. In addition to that, the spacecraft is covered with a radiation box, to create a well-defined radiation environment during the test and ease the correlation of the test results. Plate, jigs and radiation box are made of AL-6068 T6, and they are covered with Kapton tape 0.07 mm thick to bring the infrared emissivity up to 0.77.

The satellite configuration during the tests is shown in Fig. 2a, while Fig. 2b shows the configuration with the radiation box closed.

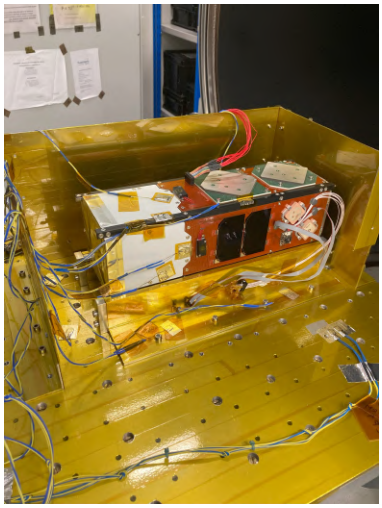

(a) CubeSat configuration inside the radiation box.

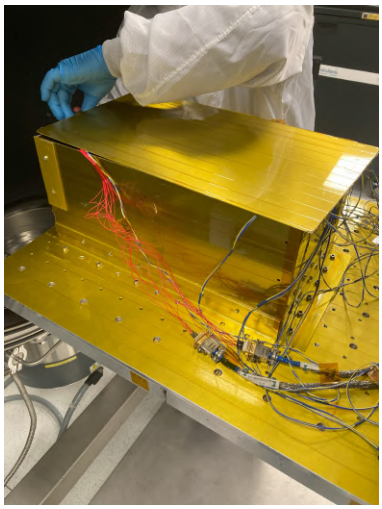

(b) View with the radiation box closed.

Fig. 2: HERMES CubeSat test configuration.

3.2 *Test setup*

To trace the temperature evolution of the CubeSat and the radiation box, a set of thermocouples is used and placed on the HERMES spacecraft, as

Copyright © 2024 by the International Astronautical Federation (IAF). All rights reserved.

shown in Table 1. The table lists the available monitoring range and accuracy for the various thermocouples.

The thermocouples from TC1 to TC14 are directly connected to the TVAC data acquisition while the all the others are acquired using the data connection with the CubeSat's OBC. Regarding the boundary conditions, two thermocouples are placed on the inner side of the radiation box, two on the top lid, and two directly on the TVAC plate. This setup provides redundancy in temperature measurements, which are used as boundary conditions during the correlation process. TC10, TC11 and TC14 are placed on the external side of the payload radiator panels, and they can be used to cross-check the measurements of the respective thermocouples on the internal side, namely TC15 and TC16.

Each thermocouple is logged every time the satellite is switched on, except for those connected to the TVAC, which can be monitored using its dedicated acquisition system throughout the entire test duration.

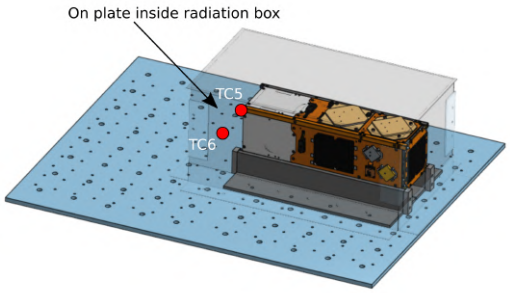

(a) TC on interface plate

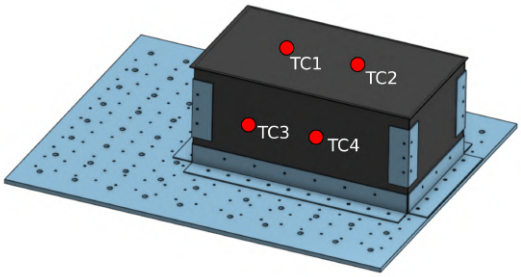

(b) TC on radiation box.

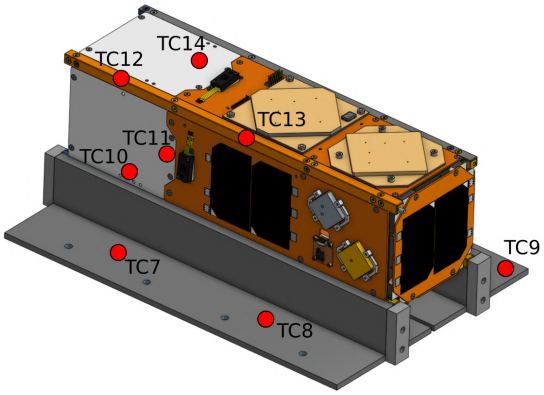

(c) TC on CubeSat.

Fig. 3: TC acquired by the TVAC data acquisition.

Copyright © 2024 by the International Astronautical Federation (IAF). All rights reserved.

TC ID	**Component**	**Min** [°C]	**Max** [°C]	**Accuracy** [°C]
TVAC interface				
TC1	Radiation Box +Y	-	-	-
TC2	Radiation Box +Y	-	-	-
TC3	Radiation Box +X	-	-	-
TC4	Radiation Box +X	-	-	-
TC5	TVAC Plate	-	-	-
TC6	TVAC Plate	-	-	-
TC7	Jig	-	-	-
TC8	Jig	-	-	-
TC9	Jig	-	-	-
TC10	Radiator +X Outside	-	-	-
TC11	Radiator +X Outside	-	-	-
TC12	Rail +X+Y	-	-	-
TC13	Rail -X+Y	-	-	-
TC14	Radiator +Y Outside	-	-	-
Panels				
TC15	Radiator +X Inside	-	-	0.5
TC16	Radiator +Y Inside	-	-	0.5
TC17	Radiator -X Inside	-	-	0.5
TC18	Radiator -Y Inside	-	-	0.5
TC19	Panel Body +X TOP	-40	85	0.5
TC20	Panel Body +X BOT	-40	85	0.5
TC21	Panel Body +Y TOP	-40	85	0.5
TC22	Panel Body +Y BOT	-40	85	0.5
TC23	Panel Body -X TOP	-40	85	0.5
TC24	Panel Body -X BOT	-40	85	0.5
TC25	Panel Body -Y TOP	-40	85	0.5
TC26	Panel Body -Y BOT	-40	85	0.5
TC27	Panel Wing -X Hinge1	-40	85	0.5
TC28	Panel Wing -X Hinge2	-40	85	0.5
TC29	Panel Wing -Y Hinge1	-40	85	0.5
TC30	Panel Wing -Y Hinge2	-40	85	0.5
TC31	Magnetometer	-40	85	1
TC32	FSS +X	-40	100	2
TC33	FSS +Y	-40	100	2
TC34	FSS -X	-40	100	2
TC35	FSS -Y	-40	100	2
Payload				
TC36	FEE -Y-X	-35	30	2
TC37	FEE +Y-X	-35	30	2
TC38	FEE +Y+X	-35	30	2
TC39	FEE +X TOP	-35	30	2
Service Module				
TC40	ACU	-35	85	2
TC41	ACU	-35	85	2
TC42	ACU	-35	85	2
TC43	PDU	-35	85	2

Copyright © 2024 by the International Astronautical Federation (IAF). All rights reserved.

TC44	P60	-35	85	2
TC45	Battery bracket	-20	60	2
TC46	Battery bracket	-20	60	2
TC47	A3200 TOP	-30	85	2
TC48	A3200 BOT	-30	85	2
TC49	A3200 Gyro	-30	85	2
TC50	GPS	-30	85	2
TC59	Magnetorquer	-40	85	2
TC60	RW	-40	80	2
TC61	IMU	-40	85	1.5
Radio				
TC51	S-Band radio	-30	60	2
TC52	S-Band radio	-30	60	2
TC53	S-Band radio	-30	60	2
TC54	S-Band radio	-30	60	2
TC55	UHF/VHF-Band radio	-30	60	2
TC56	UHF/VHF-Band radio	-30	60	2
TC57	UHF/VHF-Band radio	-30	60	2
TC58	UHF/VHF-Band radio	-30	60	2

Table 1: List of thermocouples and operational limits.

Copyright © 2024 by the International Astronautical Federation (IAF). All rights reserved.

3.3 *Test plan*

During the test, the TVAC is brought to different temperature levels. These levels are such that all the components remain within their limit temperatures, that are listed in Table 1. Specifically, the spacecraft components stay within the Operational range (Op) when the TVAC is between −10 °C and 15 °C, and within the Non-Operational range (Non-Op) when the TVAC is between −20 °C and 60 °C.

Fig. 4 illustrates the test plan, which includes one cycle in the Non-Operational range, three cycles in the Operational range, and one thermal balance cycle. The thermocouples placed on the spacecraft record data only during the Operational range cycles, as the Non-Operational one does not produce relevant data for the correlation of the thermal model. Note that the battery is charged only when the temperature is within limits.

During each thermal cycle in the operational range, the service module is activated, dissipating power and increasing the temperature. The cycle ends after a dwell time of 3 hours following the achievement of the steady state, which is defined as the point when the temperature gradient of the Thermal Reference Point (TRP) goes below 1°C h^{-1}. The TRP is assigned to the observable object with the highest mass, so that when it reaches a steady state, it can be assumed that the rest of the spacecraft has reached it as well. When the spacecraft is ON, the TRP is assigned to the reaction wheel (TC60). When the spacecraft is OFF, the TRP is assigned to the rail thermocouple (TC12), as only the thermocouples connected to the TVAC data acquisition are monitored in this state.

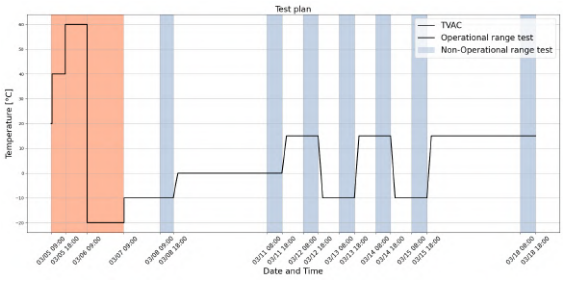

Fig. 4: PFM test plan.

4. ESATAN Model

This section presents a description of the components of the ESATAN thermal model of the HERMES CubeSat, along with the nomenclature used in the following chapters. The satellite can be divided into four groups: Panels, Payload, Service Module, and Radio. Fig. 6, 7, 8 and 9 point at the components of these groups, whose name, material and optical properties are listed in the Tables 2, 3, 4, 5 and 6.

The mechanical and optical properties of each component are taken from the datasheet provided by the manufacturer when available, otherwise they are set based on available data from literature. A full treatment can be found in [1, 3–10].

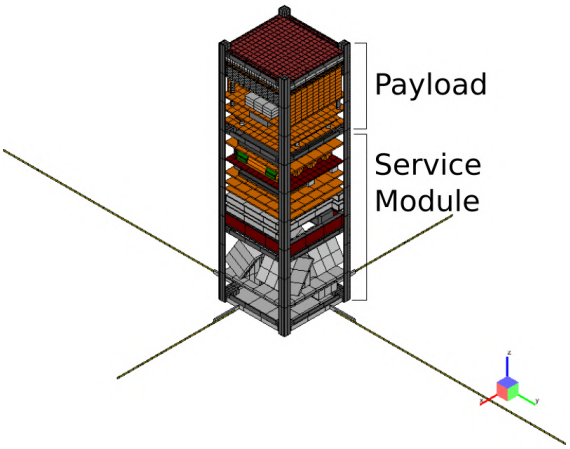

Fig. 5: HERMES Cubesat internal configuration.

Number	Component	Material	Optical
Panels			
1	Panel body	PCB	PCB
2	Radiator	Al7075	Anod Al
3	FSS	Al7075	Black paint
4	Interstage	PCB	PCB
5	S-Band RX	Patch	Patch
6	S-Band TX	Patch	Patch
7	Magnetometer	PCB	PCB
8	GPS antenna	Patch	Patch
9	Iridium antenna	Patch	Patch
10	Solar cells	Germanium	Solar cell
11	SSM	Aeroglaze	SSM

Table 2: Panels and external components materials.

Copyright © 2024 by the International Astronautical Federation (IAF). All rights reserved.

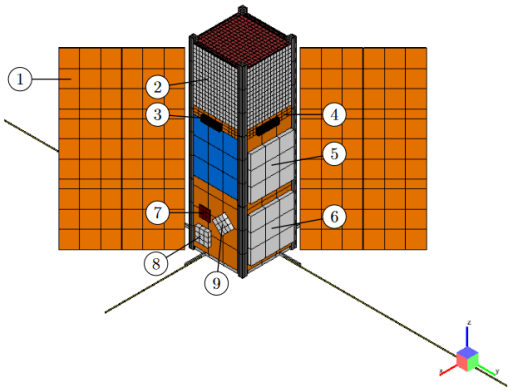

(a) Front

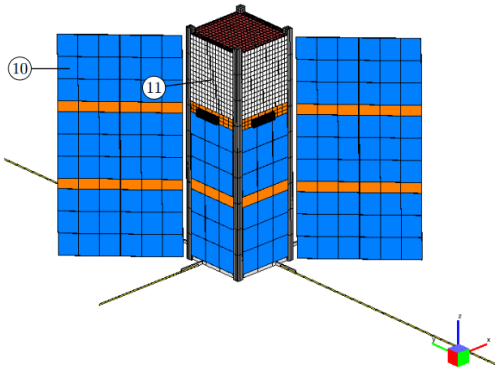

(b) Back

Fig. 6: Panels components.

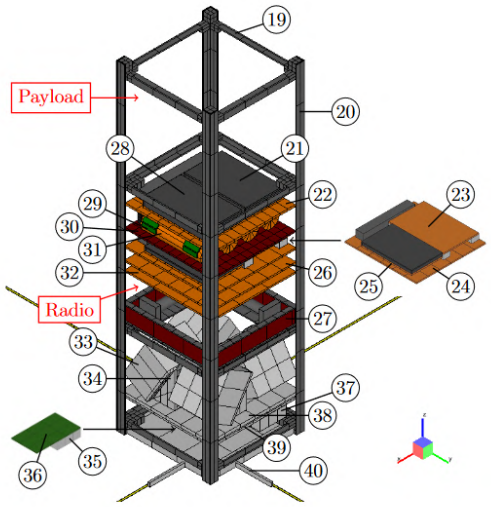

Fig. 8: Service module components.

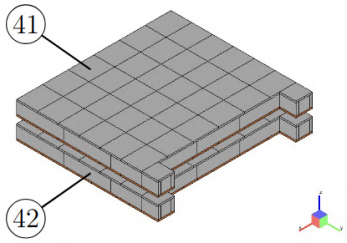

Fig. 9: Radio components.

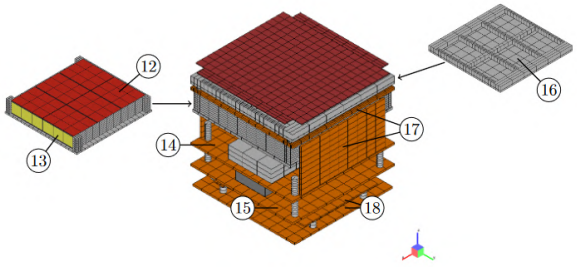

Fig. 7: Payload components.

Number	Component	Material	Optical
Payload			
12	SDD	Si	Si
13	Crystals	GAGG	Al foil
14	BEE	PCB	PCB
15	PSU	PCB	PCB
16	Optical Filter	Al1100-Kapton	MLI-Kapton
17	FEE	PCB	PCB
18	PDHU	PCB	PCB

Table 3: Payload materials.

Copyright © 2024 by the International Astronautical Federation (IAF). All rights reserved.

Number	Component	Material	Optical
Service module			
19	Rib	Anod Al	Black paint
20	Rail	Anod Al	Black paint
21	PDU	PCB	PCB
22	P60	PCB	PCB
23	GPS	PCB	PCB
24	ADCS board	PCB	PCB
25	A3200	PCB	PCB
26	Interface board	PCB	PCB
27	Magnetorquer	Anod Al-Cu	Black paint-Cu
28	ACU	PCB	PCB
29	Battery bracket	Bracket Al	Black paint
30	Battery base	PCB	PCB
31	Battery cell	Battery cell	Battery cell
32	OBC	PCB	PCB
33	RW	Al	Blank Al
34	RW base	Anod Al	Blank Al
35	Iridium modem	Al7075	Blank Al
36	Iridium interface	PCB	PCB
37	IMU	Al7075	Blank Al
38	RW shield	Anod Al	Blank Al
39	Mechanical board	Al7075	Blank Al
40	UHF/VHF antenna	Anod Al-Aramid	Anod Al-Aramid
41	UHF/VHF-Band radio	PCB	PCB
42	S-Band radio	PCB	PCB

Table 4: Service module materials.

Name	$\boldsymbol{\rho}$ [$\mathrm{kg\,m^{-3}}$]	$\mathbf{c_p}$ [$\mathrm{J\,kg^{-1}\,K^{-1}}$]	$\mathbf{k}$ [$\mathrm{W\,m^{-1}\,K^{-1}}$]
Aeroglaze	1120	2000	0.7
Al1100	2720	890	240
Al7075	2724	824	120
Anod Al	2770	900	175
Aramid	1440	1420	0.1
Bracket Al	2810	960	130
Battery cell	2810	960	130
Battery PCB	2346.3	909.56	28.25
Cu	8920	385	400
GAGG	2500	800	0.8
Germanium	5323	310	58
Kapton	1420	770	0.84
PCB	2223	589	20.3
Patch	2330	702.9	125.5
Si	2329	700	150

Table 5: Materials thermophysical properties.

Name	$\boldsymbol{\varepsilon}$	$\boldsymbol{\alpha}$
Aeroglaze	0.85	0.23
Aramid	0.9	0.9
Battery cell	0.6	0.8
Black paint	0.88	0.76
Blank Al	0.15	0.08
Cu	0.22	0.32
Kapton	0.55	0.34
MLI	0.05	0.2
PCB	0.6	0.8
Patch	0.75	0.25
Si	0.75	0.5
Solar cell	0.89	0.6
SSM	0.75	0.1

Table 6: Material radiative properties. Emissivity in the Infrared spectrum Absorptivity in the visible light spectrum.

Copyright © 2024 by the International Astronautical Federation (IAF). All rights reserved.

5. Correlation Results

This section provides a comprehensive overview of each step of the correlation process, along with the results obtained.

The correct setup of the simulation aims to recreate the PFM test conditions as accurately as possible, ensuring useful results to correlate with the model. The starting point involves modeling the HERMES CubeSat and the radiation box in ESATAN, using the configuration shown in Fig. 2 resulting in the ESATAN thermal model in the test configuration reported in Fig. 10. ESATAN automatically generates some of the conductive interfaces between the various geometries. However, this process is not entirely reliable, so all interfaces must be thoroughly checked and corrected if necessary. Additionally, user defined conductors can be employed to replace certain small elements. In the case of HERMES, all spacers inside the CubeSat and the hinges on the solar wings are replaced with UDCs.

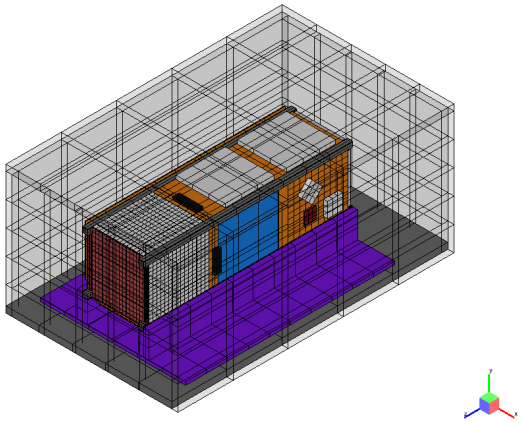

Fig. 10: ESATAN model of HERMES CubeSat and radiation box.

The temperature evolution of the radiation box is an input for the simulation. Data recorded from thermocouples TC1 to TC6 are used as boundary conditions in the model. The power dissipated by the components during the PFM test must also be considered as part of the boundary conditions. These power levels are determined by multiplying the measured voltage by the current for each component. Since the acquisition software used during the PFM test cannot record the full telemetry of power consumption, a constant value is used instead. Table 7 lists all the power levels fed into the simulation.

Finally, the initial conditions must be set, as the correlation shall be done in transient modes. These conditions are the temperature at the beginning of each test day, and they're applied to both the HERMES CubeSat and the radiation box.

In the ESATAN model, contact resistances must be manually added, indeed, the goal of the correlation process is to determine the correct values for these resistances. This is an iterative process where the results of the ESATAN simulations are compared with the data collected during the PFM test. The loop must be repeated for each component until the correlation requirements are fulfilled.

Component	**Power** [W]
Payload	
BEE	0.603
PSU	0.31
FEE top	0.045
FEE side	0.03/side - 0.06 in total
PDHU	0.429
Service Module	
PDU radio ON	1.4
PDU radio OFF	1.26
P60	0.287
GPS	1.32
A3200	0.445
Magnetorquers	0.0083
Magnetorquers coils	0.08/coil - 0.48 in total
ACU	0.287
Batteries	0.0034/cell - 0.0136 in total
OBC	0.605
IRD modem	0.105
IMU	0.825
RW	1.4/wheel - 5.6 in total
UHF/VHF antenna	0.045
Radio	
UHF/VHF-Band radio	1.042
S-Band radio	1.744

Table 7: PFM test power consumption levels.

The European Cooperation for Space Standardisation (ECSS), which develops standards for space activities, provides specific guidelines for these requirements in the document ECSS-E-ST-31C [11]. According to which the correlation is successful when:

- Temperature deviation ΔT for internal units $<$ 5K, for external units $<$ 10K;

Copyright © 2024 by the International Astronautical Federation (IAF). All rights reserved.

- Temperature mean deviation ΔT_{mean} within ±2K;
- Temperature standard deviation $\sigma < 3$K, 1σ.

However, in this paper, the first requirement is replaced with a more stringent one: ΔT must be within ±5K for both internal and external units. ΔT, ΔT_{mean} and σ are defined as:

$$\Delta T_i = T_{Mi} - T_{Pi} \quad [1a]$$

$$\Delta T_{mean} = \frac{1}{N}\sum_{i=1}^{N}(T_{Mi} - T_{Pi}) \quad [1b]$$

$$\sigma = \sqrt{\frac{1}{N-1}\sum_{i=1}^{N}[(T_{Mi} - T_{Pi}) - \Delta T_{mean}]^2} \quad [1c]$$

Where T_{Mi} is the measured temperature during the PFM test, T_{Pi} the temperature predicted by the analysis, and N is the number of samples.

At the end of the correlation process a list of contact resistances is produced. Table 8 lists the final values of all the contact resistances, which happen to be within reasonable limits available in the literature [12, 13].

For user defined conductors, the linear conductance must be calculated manually. This involves combining the two contact resistances between the UDC and the connected elements with the conductance of the replaced element. However, because the thermal resistance of the replaced element is negligible, it is omitted during the tuning process.

Note that the hinges mounted on the solar panels, which are substituted with UDCs, are not included in Table 8. Due to their complex shape, the tuning process is performed directly on the linear conductance, resulting in values of $0.01\,\mathrm{W\,K^{-1}}$ for the hinges connecting the solar panels to the CubeSat, and $0.9\,\mathrm{W\,K^{-1}}$ for the hinges connecting the two sides of each solar panel.

The remaining contact resistances are left to a reference value of $100\,\mathrm{W\,m^{-2}\,K^{-1}}$.

The deviation from the test results for the TCs on the service module is reported in Fig. 11 while for the TCs on the panels, the results are reported in the Fig. 12, except for TC1-TC6, which are used as boundary conditions thus resulting in a ΔT that is always zero.

The temperature deviation is computed for all the TCs but it is here reported only the ones of service module and panels due to layout constraints.

Object A	**Object B**	$\boldsymbol{h_c}[\mathrm{W\,m^{-2}\,K^{-1}}]$
Radiation box		
Radiation box	Jigs	1.00E+2
Jigs	Rails	2.75E+2
Panels		
Panel body	Ribs	1.00E+3
Interstage	Panel body	1.00E+3
S-Band RX	Panel body	1.00E+3
S-Band TX	Panel body	1.00E+2
Magnetometer	Panels	1.00E+4
GPS antenna	Panel body	1.00E+3
Iridium antenna	Panel body	1.00E+3
Service module		
Rails	Ribs	6.50E+4
Spacer	PCB	5.00E+3
PDU	Shield PDU	5.00E+7
PDU	P60	1.00E+4
GPS	GPS standoff	1.00E+5
GPS standoff	ADCS board	7.50E+4
A3200	Shield A3200	1.00E+7
A3200	ADCS board	1.00E+5
Magnetorquer	Ribs	1.00E+3
Magnetorquer	Coil head	1.00E+5
Coil head	Coil	1.00E+5
ACU	Shield ACU	5.00E+3
ACU	P60	5.00E+3
Battery bracket	Battery base	5.00E+3
RW	RW base	1.00E+5
RW base	RW shield	1.00E+5
RW shield	Mechanical board	1.07E+5
Mechanical board	Rib	1.07E+5
Mechanical board	IMU	1.25E+2

Table 8: Contact resistances tuned values.

Fig. 11: Deviation from test results for the TCs of the service module.

Copyright © 2024 by the International Astronautical Federation (IAF). All rights reserved.

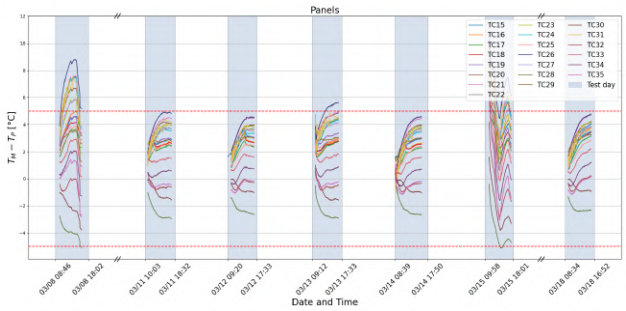

Fig. 12: Deviation from test results for the TCs of the panels.

ΔT falls within the ±5K interval for all the TCs, with minor exceptions due to the lack of knowledge about the exact location of the TCs and the absence of complete telemetry on power consumption. Nevertheless, their impact is so small that it can be neglected.

Knowing the time evolution of ΔT, it is possible to compute the mean temperature deviation ΔT_m and the temperature standard deviation σ for each thermocouple during each test day, except for March 8 and 15, when the radios are rebooted various times, making a precise correlation impossible. Subsequently, ΔT_m and σ are compared to their respective requirements. While all thermocouples meet the standard deviation requirement, most fail to meet the temperature mean deviation criterion. Indeed the temperature deviations reach a plateau in the $\pm 5\,\mathrm{K}$ range but do not approach the $\pm 2\,\mathrm{K}$ target. In these terms, better results can be achieved by continuing to tune the contact resistances. However, due to budget constraints, this approach is not pursued. The model is considered correlated, as the temperature deviation of each component remains stable within satisfactory limits.

6. Orbital Thermal Analyses

During the correlation, the thermal contact resistances are increased to match the test data. This unfortunately produced an increase in the payload temperature with respect to the non-correlated version of the thermal model.

In response, the Polimi team investigated the impact of different CubeSat attitude orientations to keep the payload as cool as possible.

At the time of writing, the Local Time of Ascending Node (LTAN) for the orbit has not been confirmed and could be either LTAN17 or LTAN1030 in a Sun-synchronous orbit (SSO) at an altitude of 550 km.

For LTAN17, there are no eclipses except between April and August. The optimal attitude to minimize payload temperature involves pointing the side opposite the payload towards the Sun for at least 40 minutes during each orbit. This reduces the intercepted solar flux, effectively creating an artificial eclipse. For the remainder of the orbit, the satellite is oriented so that only one side faces the Sun and is then adjusted to incline that side away from the Sun, further limiting solar flux input, as shown in Fig. 13 where are reported the total amount of absorbed radiative heat flux. While this allows the payload to cool down below 0°C, lower temperatures can be achieved if the side opposite the payload remains exposed to the Sun for a longer duration. Indeed, Table 9 shows the maximum and minimum temperature of each component with a 46-minutes-long maneuver. Note that, due to power requirements, the solar panels can be obscured for a maximum time of 50 minutes.

The analysis on the LTAN17 is completed with the results shown in Fig. 14, which reports the SDD temperature over one year. Specifically, the graph is obtained by linear interpolation of the data listed in Table 10. As the results show, the SDD maximum temperature never goes below 0°C, thus making necessary to create an artificial eclipse at every orbit. However, between April and August, the duration of the maneuver can be significantly lower. For example, on June 21, with a 16-minutes-long maneuver, the SDD temperature is between -5.541°C and -1.959°C.

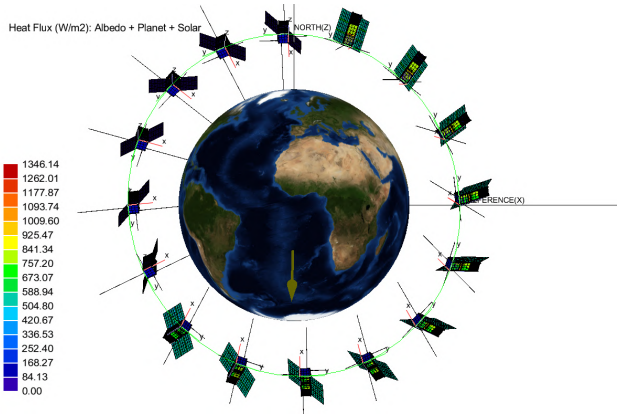

Fig. 13: LTAN17 with maneuver. Yellow arrow Sun direction.

For LTAN1030, there is an eclipse, but any maneuvers to cool the payload are constrained by the power generation system, both in time and attitude. The maximum allowable maneuvering time is 20 minutes,

Copyright © 2024 by the International Astronautical Federation (IAF). All rights reserved.

Component	T_{min}[°C]	T_{max} [°C]
A3200	19.93	30.66
ACU	23.73	37.47
ADCS dock	17.58	30.52
BEE	-6.31	7.36
Batteries	13.56	27.00
Crystals	-5.52	-1.26
FEE -Y	-10.76	2.60
FEE +Y	-8.65	1.75
FEE TOP	-5.82	-1.02
FSS	-10.75	31.09
GPS	19.87	30.59
IMU	39.79	43.50
Interface board	18.47	30.11
Iridium interface	30.75	34.96
Iridium modem	31.60	35.03
Magnetometer	7.11	13.98
OBC	19.58	31.40
Optical Filter	-5.68	-3.88
P60	8.57	32.17
PDHU	2.65	18.96
PDU	21.48	35.18
PSU	-3.76	10.05
Panels body	-48.05	68.03
Reaction wheels	32.25	38.48
S-BAND RX	-7.62	4.61
S-BAND TX	5.61	14.46
SDD	-5.34	-1.19
S-Band radio	16.93	26.89
UHF/VHF-Band radio	18.13	28.40

Table 9: Components temperature, on LTAN17 with a 46 minutes maneuver.

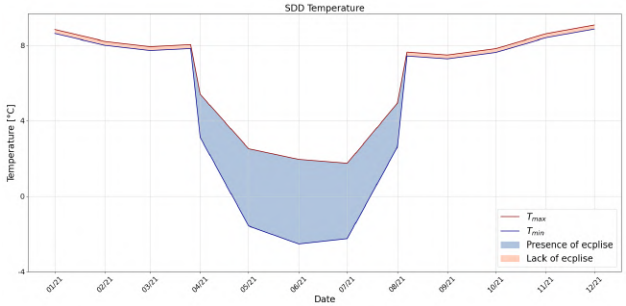

Fig. 14: SDD temperature over one year, on LTAN17.

Date	T_{min}[°C]	T_{max} [°C]	Eclipse length [min]
01/21	8.63	8.85	-
02/21	8.01	8.22	-
03/21	7.73	7.94	-
04/15	7.84	8.05	-
04/21	3.12	5.41	16
05/21	-1.57	2.53	26
06/21	-2.53	1.95	29
07/21	-2.25	1.75	26
08/21	2.60	4.9	16
08/27	7.43	7.65	-
09/21	7.28	7.49	-
10/21	7.63	7.83	-
11/21	8.41	8.62	-
12/21	8.87	9.09	-

Table 10: SDD temperature over one year, on LTAN17.

with the rest of the orbit in zenith-pointing mode. Unfortunately, this is insufficient to cool the payload well below 0 °C. The resulting attitude is reported in Fig. 15 where it is possible to see the positions of the spacecraft in which the maneuver is performed as they have a dark blue color.

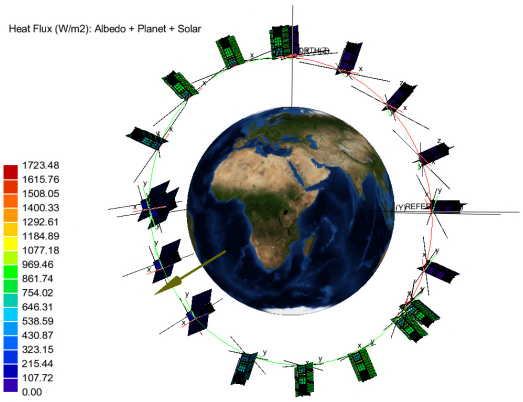

Fig. 15: LTAN1030 with maneuver. Yellow arrow Sun direction.

7. Conclusions

The HERMES mission is a pioneering effort in the use of nanosatellite constellations for astrophysical research, particularly in detecting and localizing Gamma-Ray Bursts (GRBs). This study has focused

Copyright © 2024 by the International Astronautical Federation (IAF). All rights reserved.

on the thermal modeling and testing strategy of the HERMES constellation, highlighting the key challenges and processes involved in validating the Thermal Control System (TCS) for the HERMES CubeSats.

The correlation between the thermal model and the results from the Thermal Vacuum Test (TVAC) has proven essential in confirming the reliability of the spacecraft thermal model. The modifications to thermal contact resistances produced by the correlation led to an increase in the payload temperature forcing the Polimi team to counteract this behaviour by limiting the amount of radiative input using dedicated maneuvers.

The paper reports the complete set of thermal contact resistances values produced by the correlation providing the CubeSat community with novel and precious data that can be used as starting point in the early stages of the mission design, thus providing reliable results early on.

References

[1] Yuri Evangelista, Fabrizio Fiore, Fabio Fuschino, Riccardo Campana, Francesco Ceraudo, Evgeny Demenev, Alejandro Guzman, Claudio Labanti, Giovanni La Rosa, Mauro Fiorini, Massimo Gandola, Marco Grassi, Filippo Mele, Gianluca Morgante, Paolo Nogara, Raffaele Piazzolla, Samuel Pliego Caballero, Irina Rashevskaya, Francesco Russo, Giulia Sciarrone, Giuseppe Sottile, Dorottya Milankovich, András Pál, Filippo Ambrosino, Natalia Auricchio, Marco Barbera, Pierluigi Bellutti, Giuseppe Bertuccio, Giacomo Borghi, Jiewei Cao, Tianxiang Chen, Giuseppe Dilillo, Marco Feroci, Francesco Ficorella, Ugo Lo Cicero, Piero Malcovati, Alfredo Morbidini, Giovanni Pauletta, Antonino Picciotto, Alexandre Rachevski, Andrea Santangelo, Chistoph Tenzer, Andrea Vacchi, Lingjun Wang, Yupeng Xu, Gianluigi Zampa, Nicola Zampa, Nicola Zorzi, Luciano Burderi, Michèle Lavagna, Roberto Bertacin, Paolo Lunghi, Angel Monge, Barbara Negri, Simone Pirrotta, Simonetta Puccetti, Andrea Sanna, Fabrizio Amarilli, Giovanni Amelino-Camelia, Michele Bechini, Marco Citossi, Andrea Colagrossi, Serena Curzel, Giovanni Della Casa, Marco Cinelli, Melania Del Santo, Tiziana Di Salvo, Chiara Feruglio, Fabrizio Ferrandi, Michele Fiorito, Dejan Gacnik, Gabor Galgóczi, Angelo Francesco Gambino, Giancarlo Ghirlanda, Andreja Gomboc, Mile Karlica, Pavel Efremov, Uros Kostic, Aurora Clerici, Borja Lopez Fernandez, Alessandro Maselli, Lara Nava, Masanori Ohno, Daniele Ottolina, Andrea Pasquale, Matteo Perri, Margherita Piccinin, Jacopo Prinetto, Alessandro Riggio, Jakub Ripa, Alessandro Papitto, Silvia Piranomonte, Francesca Scala, David Selcan, Stefano Silvestrini, Tomaz Rotovnik, Enrico Virgilli, Ivan Troisi, Norbert Werner, Giovanni Zanotti, Alessio Anitra, Arianna Manca, and Aurora Clerici. The scientific payload on-board the hermes-tp and hermes-sp cubesat missions. In Jan-Willem A. den Herder, Kazuhiro Nakazawa, and Shouleh Nikzad, editors, *Space Telescopes and Instrumentation 2020: Ultraviolet to Gamma Ray*. SPIE, December 2020.

[2] European Cooperation for Space Standardization. ECSS-E-ST-10-03, "Space engineering – Testing". Technical report, 2012.

[3] Matteo Quirino. Thermal analysis of HERMES-TP CubeSat using ESATAN and openFOAM. Master's thesis, Politecnico di Milano, 2019.

[4] Gianmarco D'Anna. HERMES CubeS payload thermal balance test correlation with Finite Volume Thermal Model. Master's thesis, Politecnico di Milano, 2023.

[5] Francesca Scala, Giovanni Zanotti, Serena Curzel, Mirela Fetescu, Paolo Lunghi, Michelle Lavagna, Michèle Lavagna, and Roberto Bertacin. The hermes mission: a cubesat constellation for multi-messenger astrophysics. 01 2020.

[6] Y. Evangelista, F. Fiore, R. Campana, Giulia Baroni, Francesco Ceraudo, G. Casa, E. Demenev, Giuseppe Dilillo, Massimiliano Fiorini, Giancarlo Ghirlanda, Marco Grassi, A. Guzmán, P. Hedderman, E. Marchesini, Gianluca Morgante, Filippo Mele, L. Nava, P. Nogara, A. Nuti, and N. Werner. The HERMES (High Energy Rapid Modular Ensemble of Satellites) Pathfinder mission. *ResearchGate*, September 2024.

[7] Giancarlo Ghirlanda, L. Nava, O. Salafia, F. Fiore, R. Campana, R. Salvaterra, A. Sanna, W. Leone, Y. Evangelista, Giuseppe Dilillo, S. Puccetti, A. Santangelo, M. Trenti, A. Guzmán, P. Hedderman, Gheju Camelia, Marco Barbera, Giulia Baroni, Michele Bechini, and Nicola Zorzi. HERMES: Gamma Ray Burst

Copyright © 2024 by the International Astronautical Federation (IAF). All rights reserved.

and Gravitational Wave counterpart hunter. *ResearchGate*, May 2024.

[8] Matteo Quirino, Luca Marocco, Manfredo Guilizzoni, and Michèle Lavagna. High Energy Rapid Modular Ensemble of Satellites Payload Thermal Analysis Using OpenFOAM. *J. Thermophys. Heat Transfer*, 35:1–11, March 2021.

[9] Matteo Quirino, Giulia Sciarrone, Raffaele Piazzolla, Fabio Fuschino, Yuri Evangelista, Gianluca Morgante, Manfredo Guilizzoni, Luca Marocco, Stefano Silvestrini, Fabrizio Fiore, and Michèle Lavagna. HERMES CubeSat Payload Thermal Balance Test and Comparison with Finite Volume Thermal Model. *Applied Sciences*, 13:5452, April 2023.

[10] Matteo Quirino and Michèle Lavagna. Spacecraft and Asteroid Thermal Image Generation for Proximity Navigation and Detection Scenarios. *Applied Sciences*, 14:5377, June 2024.

[11] European Cooperation for Space Standardization. ECSS-E-ST-31C, "Space engineering – Thermal control general requirements". Technical report, 2008.

[12] Philipp Hager, Tobias Flecht, Katja Janzer, Laura Leon Perez, Hugo Brouwer, and Martin Jonsson. Contact Conductance in Common CubeSat Stacks. 2019.

[13] M. Yovanovich. Four Decades of Research on Thermal Contact, Gap, and Joint Resistance in Microelectronics. *Components and Packaging Technologies, IEEE Transactions on*, 28:182 – 206, 07 2005.